Sedimentary Geology 395 (2020) 105537

Contents lists available at ScienceDirect

Sedimentary Geology

journal homepage: www.elsevier.com/locate/sedgeo

Formation and stratigraphic facies distribution of early Jurassic iron oolite deposits from west central Nevada, USA

Annaka M. Clement [a], Lydia S. Tackett [a,*], Kathleen A. Ritterbush [b], Yadira Ibarra [c]

[a] North Dakota State University, Department of Geosciences, Fargo, ND 58108, USA
[b] University of Utah, Department of Geology and Geophysics, Salt Lake City, UT 84103, USA
[c] San Francisco State University, Department of Earth and Climate Sciences, San Francisco, CA 94116, USA

ARTICLE INFO

Article history:
Received 25 July 2019
Received in revised form 7 October 2019
Accepted 9 October 2019
Available online 24 October 2019

Editor: Dr. J. Knight

Keywords:
Jurassic
Iron ooids
Ooids
Sunrise Formation
Condensation features
Panthalassa

ABSTRACT

The stratigraphic context and geochemical proxy potential are described for a newly reported early Jurassic marine iron ooid deposit in west central Nevada, U.S.A. Sedimentary analysis of the Ferguson Hill Member in the Sinemurian-aged Sunrise Formation was conducted in the Gabbs Valley Range of Nevada, U.S.A. Iron ooids were examined by transmitted light microscopy and electron scanning microscopy and found to consist of chamosite/berthierine and amorphous silica in cortical layers of the Sunrise Formation. Sedimentological characteristics of the uppermost beds of the Ferguson Hill Member show iron ooids are associated with transgressive deposits on the earliest-known first post-extinction metazoan carbonate factory identified in Eastern Panthalassa. The Ferguson Hill Member iron ooids are unique among most iron ooid deposits for being distributed grains within the carbonate. The formation of such a deposit required concentrations of iron and silica and fluctuating oxidation/reduction conditions sufficient to produce chamosite/berthierine and silica while not completely shutting down the shallow marine carbonate factory. For this reason, iron ooids observed in shallow carbonate sections serve as a useful indicator of shallow water geochemical conditions in the sedimentary record.

1. Introduction

Phanerozoic ironstones continue to interest geologists due to their economic potential, unique mineralogy, and relative rarity. Most Phanerozoic ironstones have an almost-exclusively oolitic texture, with coated grains of iron hydroxides and/or iron clay minerals (Kearsley, 1989; Van Houten, 1985; Young, 1989). Formation mechanisms for the oolitic texture remain elusive, despite many recent studies (Bhattacharyya, 1989; Kearsley, 1989; Teyssen, 1984; Van Houten, 1985; Van Houten and Purucker, 1984; Young, 1989). Although the processes that dictate the formation of iron ooids are poorly constrained, their rarity suggests that uncommon suites of geochemical conditions may be indicated by their occurrence.

The processes required for the formation of Phanerozoic iron ooids are geochemical, possibly biogeochemical, and potentially mechanical in nature. Although exact processes are not well understood and likely vary among deposits, many potential formation processes have been suggested. Iron ooids have been proposed as allochthonous grains reworked from lateritic soils (Siehl and Thein, 1989), autochthonous grains precipitating from seawater or a silicate gel (Harder, 1978), autochthonous grains formed by mechanical accretion of clay minerals (Bhattacharyya, 1983), or as a replacement of a pre-existing ooid structure (Kimberley, 1974). Most hypotheses present terrestrial weathering or volcanic input as a source of the iron, but often differ in the location and process of ooid formation (Bhattacharyya, 1983; Collin et al., 2005; Di Bella et al., 2019; Kearsley, 1989; Kimberley, 1974; Siehl and Thein, 1989; Van Houten and Purucker, 1984; Young, 1989). A biogenic origin for iron ooid nucleation and precipitation has also been proposed, including the remineralization of calcareous microfossils and the formation of iron ooids in biologically controlled environments, such as fungal mats (Dahanayake and Krumbein, 1986); although biogenic formation of iron ooids is not widely accepted (Young, 1989). While many oolitic ironstones share mineralogical, textural, or stratigraphic similarities, it appears that not all Phanerozoic ironstones share the same method of iron ooid genesis.

Attempts to define global depositional patterns in Phanerozoic oolitic ironstone deposition and distribution have not produced clear temporal or geographic trends. Phanerozoic ironstones fluctuate between periods of widespread deposition, and near or complete absence from the rock record (Van Houten, 1985). Phanerozoic oolitic ironstone deposition peaked in the Ordovician to Devonian, and again in the Jurassic to Cretaceous (Van Houten, 1985; Van Houten and Bhattacharyya, 1982; Van Houten and Hou, 1990). Very few ironstones have been reported outside of these intervals (Van Houten and Bhattacharyya, 1982). Geographic distribution also varies widely. Ordovician–

* Corresponding author.
E-mail address: lydia.tackett@ndsu.edu (L.S. Tackett).

https://doi.org/10.1016/j.sedgeo.2019.105537
0037-0738/

Devonian iron ooids accumulated during a major glaciation from 30° S to the south pole, while Jurassic–Cretaceous iron ooids primarily occurred under warm climatic conditions between 30° N and 30° S (Van Houten, 1985). The latitudinal contrast is due to the arrangement of land masses in the respective time periods; in the Devonian continents were gathered in higher paleolatitudes whereas Jurassic–Cretaceous continents were gathered in lower paleolatitudes. Thus, the iron ooid distribution demonstrates iron ooid formation is not restricted by latitude or temperature (Van Houten, 1985). Global sea level highstands, periods of continental rifting, and ocean anoxia have been proposed as drivers of iron ooid production and deposition, but only periods of significant continental shelf flooding have shown a useful correlation (Van Houten, 1985; Van Houten and Arthur, 1989).

Most studies focused on highly-concentrated deposits of iron ooids within ironstones (Young, 1989); however, iron ooids are also reported from non-ironstone deposits (Bhattacharyya, 1989; Collin et al., 2005; Ritterbush et al., 2016) and have potential uses as proxies for unique geochemical conditions in environments that may otherwise exclude the deposition of iron minerals. Here we describe the occurrence and morphology of iron ooids from a stratigraphically and geochemically well-constrained early Jurassic marine section in west-central Nevada, USA. We provide a facies model and interpret the depositional conditions that fostered iron ooid formation. In this instance, iron ooids are found in close stratigraphic proximity to shallow marine deposits containing both siliceous-sponge-derived chert, and the first post end-Triassic mass extinction metazoan-produced carbonate ramp to appear in Eastern Panthalassa (Ritterbush et al., 2014). The end-Triassic mass extinction may have been driven by ocean acidification and anoxia from degassing of large igneous provinces (Greene et al., 2012; Schaller et al., 2015; Schoene et al., 2010). Insofar as this unique combination of sedimentological features allowed the iron ooids to occur, and to be preserved, we interpret that the mass extinction interval of state-shifts and ecosystem recovery presented unique geochemical conditions for the formation of these rare clasts. With further scrutiny, the geochemical processes required to form, and to preserve, iron ooids may clarify shifting geochemical conditions in marine settings following the recovery of shallow marine environments in the early Jurassic.

2. Geologic setting

The Hettangian-Sinemurian Sunrise Formation represents one of the earliest developments of a shallow carbonate ramp following the end-Triassic mass extinction (Ritterbush et al., 2016). The ramp developed in a back-arc basin off the western coast of Laurasia in the eastern Panthalassa Ocean (Ritterbush et al., 2014, 2016; Taylor et al., 1983). early stages of recovery from the end-Triassic mass extinction were dominated by sponges extending into mid-ramp environments followed by a prograding carbonate ramp (Ritterbush et al., 2014, 2016).

The lower Sunrise Formation is well exposed in the New York Canyon area of the Gabbs Valley Range in western Nevada, USA (Fig. 1). Ritterbush et al. (2016) were the first to report iron-rich ooids in the carbonate deposits of the Ferguson Hill Member of the Sunrise Formation. The iron ooids appear to be highly stratigraphically limited, usually occurring only once per measured section in the upper portion of the Ferguson Hill Member.

3. Methods

Four new sections from the Ferguson Hill Member of the Sunrise Formation were measured in the New York Canyon area of the Gabbs Valley Range east of Luning, Nevada and are correlated with four existing measured sections from Ritterbush et al. (2016) (Fig. 1). The sections represent a modern transect of 1.94 km but, owing to large thrust faults in the Gabbs Valley Range (Ferguson and Muller, 1949), likely represent a different original distance. The facies variation seen in the Gabbs Valley Range represents km-scale variation despite the significant faulting. The transect is slightly oblique to depositional strike trending northeast-southwest. The lithology, bedding, sedimentary structures, contacts, and fossils were described in each in order to determine depositional environments. Thin-sections were made from hand-samples of some strata to aid in lithologic descriptions. From the eight total sections a composite stratigraphic cross-section was assembled and a sequence stratigraphic interpretation was made using information based on measured sections from Ritterbush et al. (2016), updated with observations from the four new measured sections.

Thin-sections of eleven beds (from New York Canyon Road and New York Canyon Gully 3) containing iron ooids were made to characterize the ooid abundance and structure using point counts. Each slide was divided into a 5 mm by 5 mm grid and a random number generator was used to select 6 sections of the slide which were then further divided into a 0.5 mm by 0.5 mm grid. Every intersection on the 0.5 mm by 0.5 mm grid was counted for each of the 6 sections for a total of 1200 points per slide. For each ooid (iron or calcite) counted, length, width, core lithology, core angularity, and surface abrasion were also recorded. The Powers standard was used for qualitative core grain angularity (Powers, 1953), and a qualitative scale from 0 to 3 (0 - no abrasion, 1 - slight surface abrasion that does not significantly impact laminae, 2 - moderate surface abrasion or deformation that does impact laminae, 3 - severely abraded, deformed, and/or broken) was used for surface abrasion. Thin-section analysis and imaging was done using a Zeiss Discovery.V12 with Zeiss Zen Pro software and imaging.

Imaging and energy-dispersive X-ray analysis (EDXA) with a scanning electron microscope (SEM) was conducted to characterize the composition and morphology of the ooid laminae. Billets cut from iron ooid-rich samples from Reno Draw and New York Canyon Road were polished by hand to 5 μm using glass slides and wet carborundum grit. Billets from New York Canyon Road and New York Canyon Gully 3 were likewise polished then etched with 10% HCl for 10 s. Polished and etched specimens were attached to cylindrical aluminum mounts with conductive carbon adhesive tape or Leit-C-Plast carbon mounting putty (Ted Pella, Redding, California, USA), and then sputter coated (Cressington 108auto, Ted Pella, Redding, California, USA) with a conductive layer of gold. Images were obtained with a JEOL JSM-6490LV scanning electron microscope (JEOL USA, Inc., Peabody, Massachusetts USA) at an accelerating voltage of 15 kV.

Energy-dispersive X-ray information was collected at an accelerating voltage of 15 kV using a ThermoScientific UltraDry Premium silicon drift detector with NORVAR light element window and Noran System Six imaging system (ThermoFisher Scientific, Madison WI, USA). Scans were conducted by the NDSU Electron Microscopy Center.

4. Depositional facies and model

Four facies are present in the Ferguson Hill Member of the Sunrise Formation in the New York Canyon area of the Gabbs Valley Range in Nevada; interbedded chert and carbonate (ICC), oolitic carbonate (OC), skeletal lime-mudstone to grainstone (SLMG), and coral wackestone to packstone with oncolite layers (CWPO). Facies are defined based on their lithology, bedding, fossils, and relationship to other facies (Table 1).

4.1. Interbedded chert and carbonate (ICC)

Facies ICC contains interbedded chert and skeletal/peloidal wackestone–grainstone beds. Chert beds contain undamaged in situ siliceous sponge spicules as well as minor amounts of micrite, peloids, and micritized shells. The tops of some chert beds contain whole sponge

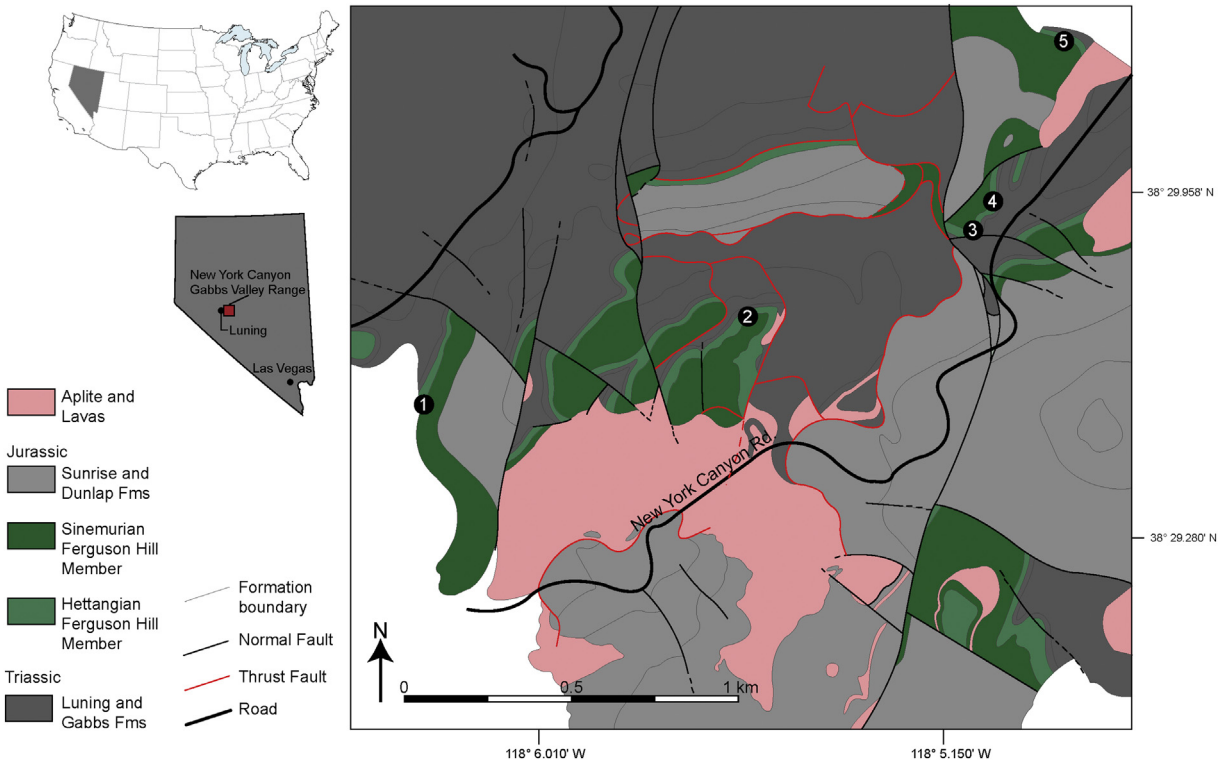

Fig. 1. Geologic map of New York Canyon, Gabbs Valley Range, Nevada, U.S.A. Geologic map based on Ferguson and Muller (1949). Ferguson Hill Member strata are highlighted in green. Measured section locations are indicated by numbers. (For interpretation of the references to color in this figure legend, the reader is referred to the web version of this article.)

body fossils. Skeletal/peloidal wackestone–grainstone beds contain abundant broken spicules in addition to weathered shell material and occasional peloids. Wackestone–grainstone beds are well-sorted and contain grains of skeletal fragments from lower fine sand to very coarse sand. The chert and carbonate beds are thin to medium bedded and contacts between the two are sharp and often irregular. Facies ICC has a gradational upper contact with facies SLMG observed in measured section Dip Slope (2). Iron ooids were not observed in facies ICC.

4.1.1. Interpretation

Facies ICC is interpreted to represent a mid-ramp environment. Ritterbush et al. (2014) outlined how sponge-dominated communities moved into mid-ramp settings, producing biosiliceous (originally opal) layers interbedded with carbonate (cropping out now as interbedded chert and carbonate). The thin skeletal/peloidal wackestone–grainstone beds are interpreted to be storm deposits based on the weathered allochthonous grains and the well-sorted nature (Burchette and Wright, 1992; Ritterbush et al., 2016). Facies ICC is equivalent to those described as representing Middle to Inner Ramp deposits in Ritterbush et al. (2016).

4.2. Oolitic carbonate (OC)

Ooid-bearing facies OC contains calcite ooid-rich lime-mudstone, wackestone, packstone, and grainstone beds. Bedding is medium to thin and no sedimentary structures were observed within the beds. Packstone and grainstone beds are poorly to well sorted. The calcite ooids may be a calcite mosaic with a micritized rim or are composed

Table 1
Facies of the Ferguson Hill Member of the Sunrise Formation.

Facies	Sedimentology	Paleontology	Contact relationships
ICC: Interbedded chert and carbonate (mid-ramp)	Thin to medium interbedded well-sorted peloidal wackestone–grainstone beds and dark weathering chert.	Reworked sponge spicules are common in wackestone–grainstone beds. Calcite skeletal fragments are common and often micritized.	Contacts between the wackestone–grainstone beds and the interbedded chert are often irregular. Conformably underlies facies OC
OC: Oolitic carbonate (shoal)	Thin to medium bedded oolitic lime-mudstone, wackestone, packstone, and grainstone beds. Packstone and grainstone beds are poorly to well sorted. Ooids may be a calcite mosaic with a micritized rim or have tangentially oriented carbonate laminae.	Rare bivalve skeletal fragments.	Iron ooids occur only near the tops of measured sections. Erosive lower contact, but conformably overlies facies ICC. Gradational top contact with facies SLMG.
SLMG: Skeletal lime-mudstone–grainstone (distal inner-ramp)	Medium to thick bedded, poorly-sorted skeletal wackestone to grainstone beds.	Bioclasts are often partially or completely micritized. Bioclasts include whole and fragmentary gastropods, crinoids, other echinoids, infaunal bivalves.	Gradational lower contact with facies OC and facies ICC. Gradational upper contact with facies CWPO.
CWPO: Coral wackestones–packstones with oncolite layers (proximal inner-ramp and patch reef)	Thin–medium bedded skeletal wackestone–packstone beds containing coal and oncolites. Beds may locally contain peloids.	Bioclasts include coral and whole to fragmentary gastropods, echinoids, and infaunal bivalves.	Gradational lower contact with facies CWPO.

of tangentially oriented carbonate laminae. Facies OC rarely contains shell skeletal fragments. The base of beds forms a slightly erosive contact, but the facies has a gradational upper contact with facies SLMG.

4.2.1. Interpretation

Facies OC is interpreted to represent shoal deposits. The formation of calcite ooids requires constant agitation and often form in and aggregate in shallow areas where environments with high and low turbulence are adjacent (Simone, 1981), such as at the fair weather wave base or in tidal settings (Burchette and Wright, 1992). The oolitic lime-mudstone, wackestone, packstone, and grainstone deposits of the Ferguson Hill Member are usually less than a meter in total thickness and do not show internal sedimentary structure characteristic of many tidal ooid deposits (Burchette and Wright, 1992; Rankey et al., 2006). For this reason and the gradational upper contact with facies SLMG, the oolitic carbonates are considered a grain shoal developing between the mid- and inner-ramp at fair weather wave base. Facies OC is considered to conformably overlie facies ICC based on its stratigraphic position in measured sections. Iron ooids are only found in facies OC near the tops of the measured sections. Iron ooids are often found interspersed with calcite ooids and with calcite layers within their structure, suggesting they potentially formed or accumulated in a similar environment. Facies OC is equivalent to those described as representing Coarse-Grained Shoal deposits in Ritterbush et al. (2016).

4.3. Skeletal lime-mudstone to grainstone (SLMG)

Facies SLMG contains medium to thick bedded skeletal lime-mudstone to grainstone beds. The lime-mudstone to grainstone beds are poorly-sorted and contain primarily bioclastic grains. Bioclasts include whole and fragmentary gastropods, crinoids, other echinoids, and burrowing bivalves. No sedimentary structures are observed in the field, although infaunal bivalves are present. Fossils are often partially to completely micritized. Facies SLMG has a gradational lower contact with facies OC and a gradational upper contact with facies CWPO. In one measured section (Dip Slope 2) facies SLMG is observed to have a gradational lower contact with facies ICC. Iron ooids are only observed in this facies near the tops of measured sections.

4.3.1. Interpretation

The skeletal lime-mudstone–grainstone beds of facies SLMG represent an open shallow subtidal environment such as the distal portion of the inner-ramp (Ritterbush et al., 2016). The abundance of bioclasts and bioturbation, suggested by the presence of burrowing bivalves and lack of sedimentary structures, supports this interpretation (Burchette and Wright, 1992; Tucker, 1985). This facies is interpreted to be more landward than the interbedded chert and skeletal/peloidal wackestone–grainstone beds owing to the intact nature of many fossils and the gradational lower contacts with facies OC and ICC. Facies SLMG is equivalent to those described as representing the Inner Ramp deposits of the Inner Ramp to Lower Shoreface Transition described in Ritterbush et al. (2016).

4.4. Coral wackestone to packstone with oncolite layers (CWPO)

Facies CWPO contains skeletal wackestone to packstone beds that frequently contain corals and oncolites. Facies CWPO is thin to medium bedded and the bioclasts include whole to fragmentary gastropods, echinoids, and infaunal bivalves, and in some beds whole coral. The scleractinian coral preserved in some facies CWPO is relatively small (up to 3 cm) and solitary. There is no sign of significant bounding or reef-building. The matrix around fossils can be locally peloidal. Facies CWPO also contains packstone to rarely grainstone beds with oncoids as the primary grain. The oncolites layers can also contain peloids and coated skeletal grains. Facies CWPO has a gradational lower contact with facies SLMG.

4.4.1. Interpretation

Facies CWPO is interpreted to be proximal inner-ramp deposits. The similar lithology and fossil assemblage to facies SLMG as well as their close stratigraphic association supports facies CWPO's interpretation as an inner-ramp deposit. Beds with many small solitary corals but no significant bounding structures suggest the presence of shallow patch reefs or reef mounds (Tucker, 1985). The gradational lower contact with facies SLMG indicates facies CWPO is more landward. Oncoids are observed to form in tidal pools and peritidal settings in modern environments (Basso et al., 2012). The oncoids in facies CWPO likely formed in an adjacent tidal to peritidal environment not preserved in the Ferguson Hill Member rocks in New York Canyon, but oncoids were exported and preserved in the wackestone and packstone beds of the inner-ramp facies. The presence of oncoids in facies CWPO supports its interpretation as the most landward facies preserved in the Ferguson Hill Member. Iron ooids are only observed in facies CWPO at the tops of measured sections. Facies SLMG is equivalent to those described as representing the Lower Shoreface Transition deposits of the Inner Ramp to Lower Shoreface Transition described in Ritterbush et al. (2016). The Ramp Termination facies is no longer recognized as a unique facies in the model.

4.5. Depositional model

In this work, the depositional model is simplified from the three progressive Hettangian–Sinemurian models from Ritterbush et al. (2016) into a single carbonate ramp with biosiliceous input. Facies variations in the Ferguson Hill Member in New York Canyon interpreted to be deposition in the mid to inner-ramp portion of a carbonate ramp (Tucker, 1985) based on lithology, bedding, fossil accumulations, sedimentary structures, and facies stratigraphic relationships (Fig. 2). All four facies have gradational vertical relationships indicating laterally adjacent depositional environments along a depth transect (Middleton, 1973), with the exception of the base of facies OC (oolitic carbonates) which has a sharp, likely erosive, base.

Facies ICC (interbedded chert and carbonate) represents the most distal facies. Peloidal wackestone–grainstone beds indicate deposition in quiet subtidal water and the spicule-rich chert suggests a deeper mid-ramp environment dominated by sponges adjacent to the shallower carbonate facies (Ritterbush et al., 2016). The boundaries between the chert and carbonate are sharp and often irregular likely owing to the migration of silica. Facies ICC is sharply overlain by a facies OC (discontinuous oolitic carbonate shoal) or gradationally by facies SLMG (distal inner-ramp environments). Despite the erosive base of

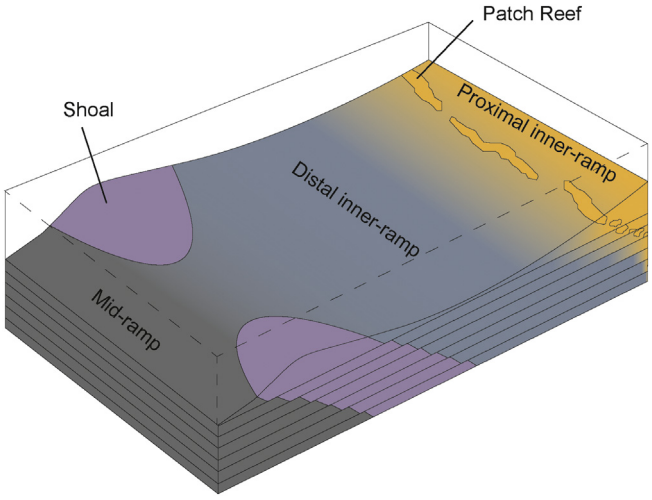

Fig. 2. Facies model diagram representing the Sinemurian upper Ferguson Hill Member strata.
This model is adapted from Ritterbush et al. (2016).

facies OC, the gradational transition from facies ICC into facies SLMG, and from facies OC vertically into facies SLMG, indicate the discontinuous oolitic deposits separate facies ICC (mid-ramp environments) from facies SLMG (Fig. 2). The lack of internal sedimentary structures and thin bedding in facies OC indicates they were more likely to be the result of agitation near fair-weather wave base rather than tidal environments (Burchette and Wright, 1992; Rankey et al., 2006). Skeletal lime-mudstone to grainstone beds of facies SLMG are gradationally overlain by coral wackestone to packstone interbeds with oncolite layers of facies CWPO (proximal inner-ramp environment). The gradation between facies SLMG and CWPO is subtle and not easily discerned until coral fossils or oncoids are identified. Facies CWPO also occurs with differing frequency in very closely spaces columns in New York Canyon. The subtle gradation and varying frequency indicate facies CWPO is more likely a series of small patch reefs or reef mounds lining the inner-ramp rather than a large platform reef. Viewed together, the facies describe deposition along the mid to inner-ramp of a mixed carbonate-siliciclastic ramp.

This facies model agrees well with the models proposed by Ritterbush et al. (2014, 2016). This model combines and refines the previous models into a single system. Removing iron ooids as a distinct facies and considering the cherts as the most distal facies in this shallow system allows for a single facies model to represent the early Sinemurian.

5. Iron ooid description and analysis

5.1. Abundance and distribution

Iron ooids are restricted to the uppermost portion of the Ferguson Hill Member, with the exception of Reno Draw, but are found in most facies present in the uppermost Ferguson Hill Member (facies OC, SLMG, and CWPO). Iron ooids were found in five of the eight columns (Reno Draw, New York Canyon Road, New York Canyon Gully 1, New York Canyon Gully 2, and New York Canyon Gully 3) (Fig. 3). Two iron ooids were found in thin-sections from mid-column at Reno Draw. Both ooids were broken and highly abraded. Owing to these factors, the ooids were not considered for further analysis. The abundance and preservation condition of the iron ooids varies (Table 2).

Ooid abundance and preservation vary within and among facies (Table 2). Facies CWPO and SLMG, interpreted as distal and proximal inner-ramp environments respectively, have the most abundant iron ooids, 0–8.83% of grains in CWPO and 0.5–11.5% of grains in SLMG in a 1200-point count. Iron ooids are also found in facies OC at lower abundances of 0–1.5%. No evidence of iron ooids was found in facies ICC.

Some iron ooids display signs of transport including breakage and abrasion (Fig. 3c, d). Iron ooids retain their internal structure when damaged, even when highly deformed or broken apart. The most damaged ooids are found in facies OC (New York Canyon Road). All facies display a range of iron ooid breakage and abrasion (Table 2).

5.2. Size and shape

From thin-section analysis, iron ooids range in size from major axis measurements of 136 to 684 μm and minor axis measurements of 81 to 567 μm. The average major axis length is 377 μm and average minor axis length is 233 μm (Table 2). The average major to minor axis ratio, or obliquity, is 1.62. Three-dimensional shape is difficult to extrapolate from thin-section, so extracted ooids were used to classify shape.

Based on iron ooid extractions ($n = 128$), iron ooids were observed to fall into three shape categories: oblate, prolate, and triaxial (Figs. 4, 5). An obliquity value of 1.2 (length/width) was selected for the cutoff between oblate ooids and prolate and triaxial ooids because the long axis could be recognized on sight. A value of 1.2 for the width/height was also used to separate triaxial (width/height ≥ 1.2) from prolate ooids (width/height < 1.2). In total, 54% of iron ooids are triaxial with length ranging from 309 to 748 μm, width from 228 to 581 μm, and height from 143 to 362 μm. Oblate ooids were also common (38%) with diameters (length and width) from 217 to 623 μm and heights from 207 to 329 μm. True prolate ooids were comparatively rare (8%) with lengths ranging from 257 to 560 μm and widths from 169 to 333 μm.

5.3. Iron ooid structure and composition

In thin-section, iron ooids appear as ovals with distinct light and dark cortical laminae in plane-polarized and cross-polarized light (Fig. 3a, b). Laminae thicken along the long axis and rarely show significant asymmetry on either side of the core. This is indicative of their three-dimensional shapes as primarily oblate and triaxial, most planes cut through these ooid shapes would result in only minor asymmetry. Most light laminae in thin-section exhibit low-order birefringence and low relief under cross-polarized light and are identified as quartz or amorphous silica (glass) (Fig. 3e). Some light laminae are carbonate in composition and show typical high order birefringence in cross-polarized light (Fig. 3f). Dark laminae appear primarily opaque gray to black in plane-polarized and cross-polarized light and do not change under cross-polarized light. Dark laminae may appear slightly silver under cross-polarized light when the stage is rotated (Fig. 3a, b). Core material is varied and includes angular to rounded particles of chert, quartz, calcite, micrite, iron oxide, potential peloids, and rarely fossil fragments (Fig. 3a–f).

Cortical laminae are also visible in whole extracted iron ooids. In broken iron ooids, laminae are visible with a 10× hand lens. In direct rather than transmitted light the true colors are visible. The iron-rich laminae are opaque light tan to white. Silica and calcite layers are indistinguishable from one another in direct light and both appear as clear to translucent colorless laminae.

In SEM analysis silica and iron rich laminae are much less distinct and display an irregular clotted texture of iron rich and silica rich compositions (Fig. 6a). The clotted texture is best observed in polished samples. Laminae do not show a dominantly radial or tangential crystal orientation (Fig. 6a, b). Calcite laminae do not show the clotted texture and remain distinct and visible in etched samples (Fig. 6b).

The composition of iron-rich laminae was investigated during SEM structural analysis using energy-dispersive X-ray analysis (EDXA). Laminae interpreted to be iron-rich in thin section (based on opacity in plane-polarized light and cross-polarized light, Fig. 3) contained electromagnetic emission peaks consistent with iron, magnesium, silicon, oxygen, aluminum, and occasionally titanium indicating an iron/-magnesium aluminosilicate such as chamosite or berthierine (Fig. 6d). Laminae identified as silica in thin section were dominated almost entirely by silicon and oxygen, confirming the identification (Fig. 3c). Grains containing primarily phosphorus, calcium, and oxygen were also observed in EDXA, indicating the presence of apatite (Fig. 3e).

5.4. Summary and interpretation

Iron ooids can be easily distinguished from their calcite counterparts based on their shape, structure, and composition. Iron ooids from the Ferguson Hill Member are distinctly ovate and usually triaxial or oblate in shape. Individual laminae in iron ooids are thickened along the longest axis, resulting in an elongate appearance distinct from the more common spherical calcite ooids. The structure and compositional differences can also be readily observed in thin-section. Iron ooids display contrasting light and dark laminae that are distinct and readily identifiable. Iron-clay rich laminae appear dark, opaque, and unchanging in plane-polarized and cross-polarized light and light-colored laminae can be identified as silica or calcite under cross-polarized light. With SEM and EDXA analysis, the iron-rich composition of the iron-clay

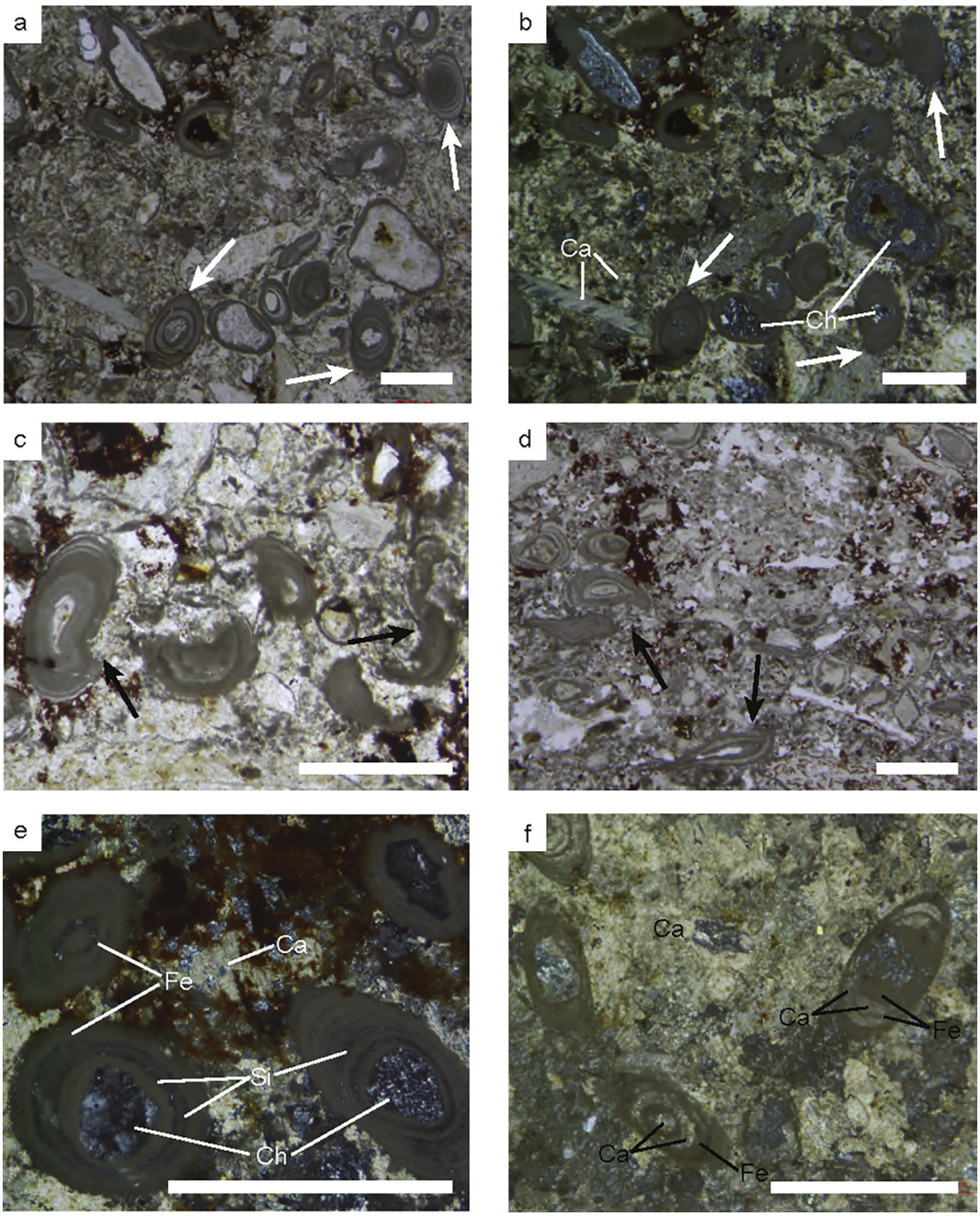

Fig. 3. Thin section images of iron ooids. All scales 0.5 mm. Labels: Fe - iron-clay, Ca - calcite, Ch - chert, Si - amorphous silica (a–b) Iron ooids with distinct calcite and chert cores. Long axes show thickened laminae indicated by white arrows (New York Canyon Gully 3 sample 7b). (a) plane-polarized light. (b) cross-polarized light. (c) Broken and deformed iron ooids showing intact laminae as primary structures. Black arrows indicate deformed areas. Black arrows indicate deformed ooids. (New York Canyon Gully 3 sample 6c). (d) Iron ooids with intact laminae showing some bedding parallel deformation (NYC Rd 6Ua). (e) Iron ooids with alternating laminae of opaque iron-clay mineral and low order birefringence silica (NYC Gully 3 sample 7a). (f) Iron ooids with alternating laminae of opaque iron-clay mineral and high order birefringence calcite (NYC Road sample 6NSa).

(chamosite or berthierine) can be determined and the clotted microstructure of the iron-clay and silica layers is revealed.

6. Discussion

6.1. Stratigraphy

The upper portion of the Ferguson Hill Member in the Sunrise Formation represents a shallowing-upward package of mostly carbonate rocks with a combined sequence boundary and transgressive surface near the top of the measured sections (Fig. 7).

The upper part of the Ferguson Hill Member begins with clear progradational stacking of facies above a potential maximum flooding surface (Fig. 7). The maximum flooding surface is defined by the greatest concentration of chert in facies ICC, indicating the largest contribution of sediments by mid-ramp sponges. Above this surface, carbonate contribution dominates silica, shown in the progradation of facies SLMG and CWPO (interpreted as inner-ramp deposits). Facies ICC (interpreted as mid-ramp) is overlain with facies OC (interpreted as a shoal separating the mid- and inner-ramp deposits) and occasionally facies SLMG (interpreted as distal-inner-ramp). Facies SLMG gradationally overlies both facies ICC and facies OC. Facies SLMG grades vertically into facies CWPO (interpreted as proximal inner-ramp and

Table 2
Results of iron ooid point counts. Percentage iron ooid grains based on 1200 points recorded per sample. Level of abrasion assessed with a qualitative scale from 0 to 3 (0 - no abrasion, 1 - slight surface abrasion that does not significantly impact laminae, 2 - moderate surface abrasion or deformation that does impact laminae, 3 - severely abraded, deformed, and/or broken).

Sample	% iron ooids	Average major axis (mm)	Average minor axis (mm)	Average obliquity (major/minor axis)	Average abrasion	Core angularity & composition	Lithology	Facies
NYC G3 2a	4.3%	0.397	0.234	1.70	1.41	Rounded-iron clay	Skeletal/iron ooid wackestone–packstone.	Distal inner ramp
NYC G3 3a	5.7%	0.365	0.212	1.72	1.52	Rounded-variable, micrite	Skeletal/iron ooid wackestone–packstone with coral fossils. Ooids have blebby layers and calcite grains included.	Proximal inner ramp
NYC G3 4a	3.7%	0.366	0.248	1.47	1.59	Rounded-variable, micrite, iron clay, calcite, and quartz	Skeletal/iron ooid wackestones.	Distal inner ramp
NYC G3 6c	8.8%	0.391	0.257	1.52	1.31	Rounded-iron clay and subrounded to angular-calcite and chert	Skeletal/iron ooid wackestone–grainstone with large almost complete fossils including coral. Iron ooids in good condition.	Proximal inner ramp
NYC G3 7b	11.5%	0.371	0.230	1.61	0.90	Rounded-angular primarily calcite	Iron ooid/intraclastic wackestone with some large skeletal fragments and areas of sparry cement and many quartz grains.	Distal inner ramp
NYC Rd (J) 2a	1.5%	0.398	0.244	1.63	2.0	Rounded-iron (probably all oblique cuts)	Skeletal/peloidal wackestone with some calcite ooids.	Shoal
NYC Rd (J) 3a	0.0%	N/A	N/A	N/A	N/A	N/A	Calcite ooid/skeletal wackestone–packstone. Calcite ooids only have 1–2 layers.	Shoal
NYC Rd (J) 4a	0.5%	0.427	0.229	1.86	1.67	Rounded-iron (probably all oblique cuts)	Calcite oolitic mudstone. Ooids only have 1–2 layers. The matrix is notably red/brown.	Distal inner ramp
NYC Rd (J) 5a	0.0%	N/A	N/A	N/A	N/A	N/A	Skeletal/calcite ooid packstone that contains the oncoid layer. Matrix is notably reddish/brown.	Proximal inner ramp
NYC Rd (J) 6NSa	1.0%	0.334	0.176	1.90	1.33	Rounded-iron clay (probably all oblique cuts)	Calcite ooid/skeletal wackestone–grainstone with large complete fossils. Contains a few well-intact iron ooids.	Shoal
NYC Rd (J) 6Ua	1.0%	0.424	0.192	2.21	1.17	Angular to rounded-iron clay	Skeletal/calcite ooid wackestone–packstone. Iron ooids have blebby layers and are often deformed.	Shoal

patch reef) (Fig. 7). Parasequences quickly lose facies OC following the maximum flooding surface and gain the shallowest facies (CWPO) near the middle of the sections. This shallowing-upwards package is capped by an abrupt return of facies OC and SLMG, indicating a major flooding surface. Above the flooding surface, bedding is thin to medium and parasequences are thin. At Reno Draw, where the measured section was not cut off by a fault, facies SLMG and the carbonates from facies ICC persist up section and stack retrogradationally. The progradational stacking of facies ICC, OC, SLMG, and CWPO above a maximum flooding surface followed by the return of deeper facies defines the highstand systems tract.

The surface defined by the shift from progradational to retrogradational stacking is the basinward extension of a sequence boundary and the transgressive surface (Fig. 7). The change in stacking pattern defines the transgressive surface as facies deepen upward to facies ICC (interpreted as mid-ramp) above the transgressive surface. There is no evidence of subaerial exposure in the sections measured in the New York Canyon area; instead, the change from shallowing upward to deepening upward necessitates a landward sequence boundary along with the transgressive surface. The correlative conformity and transgressive surface is subtle in the field. Beds are thinner and return to deeper facies immediately above the inferred surface.

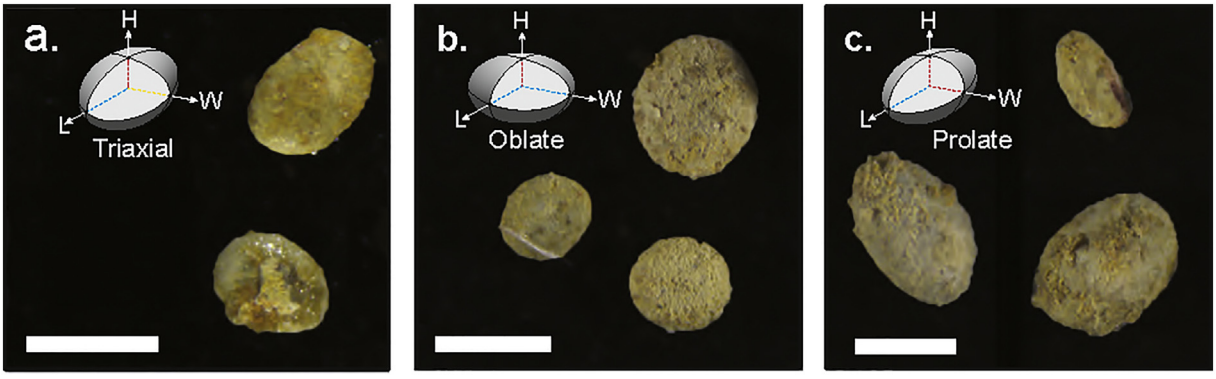

Fig. 4. Extracted iron ooids. Iron ooid primary shapes extracted from carbonate matrix using acetic acid. Inset diagrams show orientation of primary axes measured. L - length, W - width, H - height. All scales 0.5 mm. (a) Triaxial ooids looking down the H (height) axis. L, W, and H are all different lengths. (b) Oblate ooids looking down the H (height) axis. L and W are approximately equal (c) Prolate ooids looking down the H (height) axis. H and W are approximately equal.

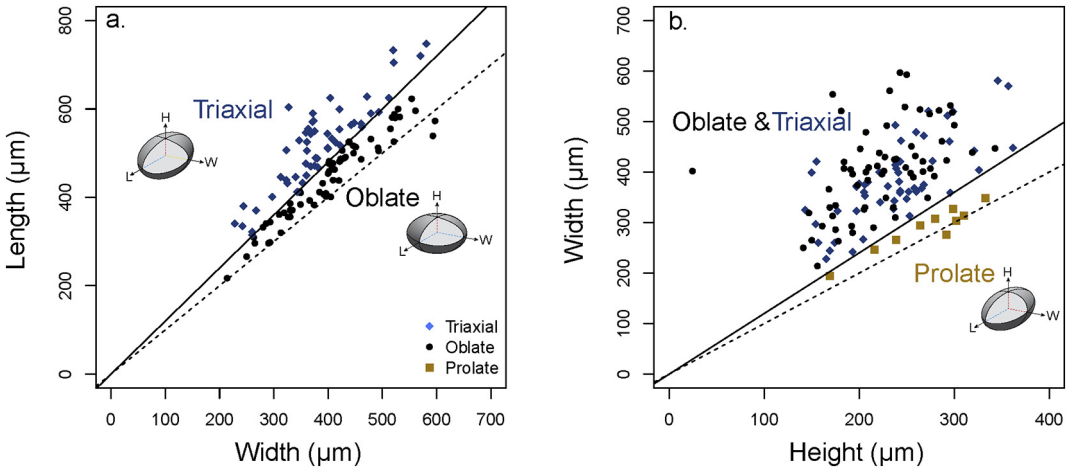

Fig. 5. Iron ooid shape differentiation. Plots indicating the length, width, and height ratio cut-offs for triaxial, oblate, and prolate iron ooids. Dashed lines have a slope of 1. Solid lines indicate the 1.2 obliquity cut-off for shape categories. (a) Length vs. width plotted for triaxial and oblate ooids. (b) Width vs. height plotted for triaxial, oblate, and prolate ooids.

Above the transgressive surface in the transgressive systems tract, facies stack retrogradationally, deepening upwards into facies ICC (Fig. 7). Iron ooids are found within the transgressive systems tract, usually just above the transgressive surface. The iron ooids are found preserved in all facies indicating that, while they may have a preferred formation environment, they are better-described as a condensation feature. The overlying Five Card Draw Member of the Sunrise Formation is described at its base as siliceous siltstone and mudstone containing ammonites (Taylor et al., 1983), suggesting that facies continue to shift basinward to more open water settings that potentially lack strong input from siliceous sponges.

6.2. Iron ooids as stratigraphic condensation features

Iron ooids in the Ferguson Hill Member are found in multiple facies in a stratigraphic interval of thinly bedded backstepping shallow marine carbonates. Their accumulation in a single stratigraphic interval across the study area within the transgressive systems tract supports their interpretation as a condensation feature. Stratigraphic condensation occurs at very low sedimentation rates resulting in a stratigraphically thinner deposit than a contemporaneous standard (Heim, 1934; Föllmi, 2016). Low sedimentation rates over extended periods of time allow for relatively rare elements, such as iron, to accumulate and represent a much larger proportion

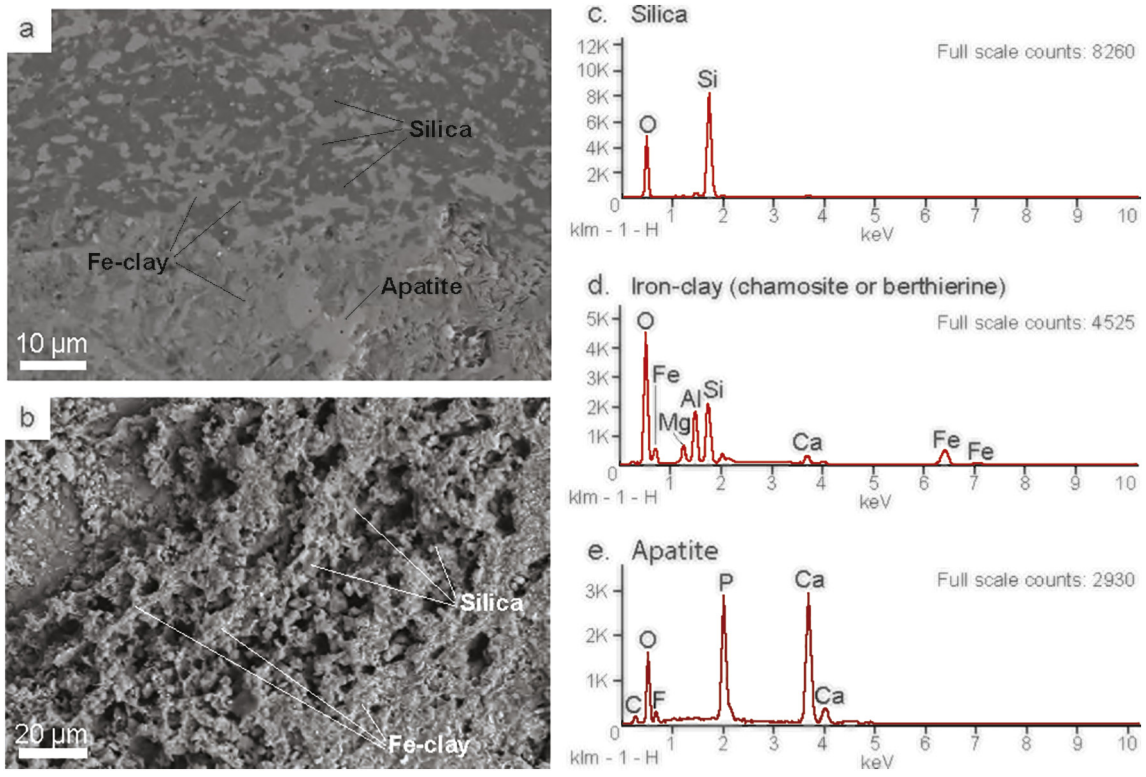

Fig. 6. SEM images and EDXA results from image a. (a) SEM image of a polished iron ooid showing a clotted texture with silica and iron-clay dominated regions. (b) SEM image of an etched iron ooid showing silica and iron-clay dominated regions that have not been affected by etching. Iron-clay, while in discernible cortical layers, does not appear to have a preferred orientation and is mixed with silica. (c) EDXA results plot showing peaks for silicon and oxygen indicating the presence of silica. (d) EDXA results plots showing peaks for oxygen, iron, magnesium, aluminum, silicon, and calcium indicating the presence of an iron/magnesium-rich clay mineral such as chamosite or berthierine. (e) EDXA results plot showing peaks for carbon, oxygen, fluorine, phosphorus, and calcium with major peaks for oxygen, phosphorous, and calcium indicating the presence of apatite.

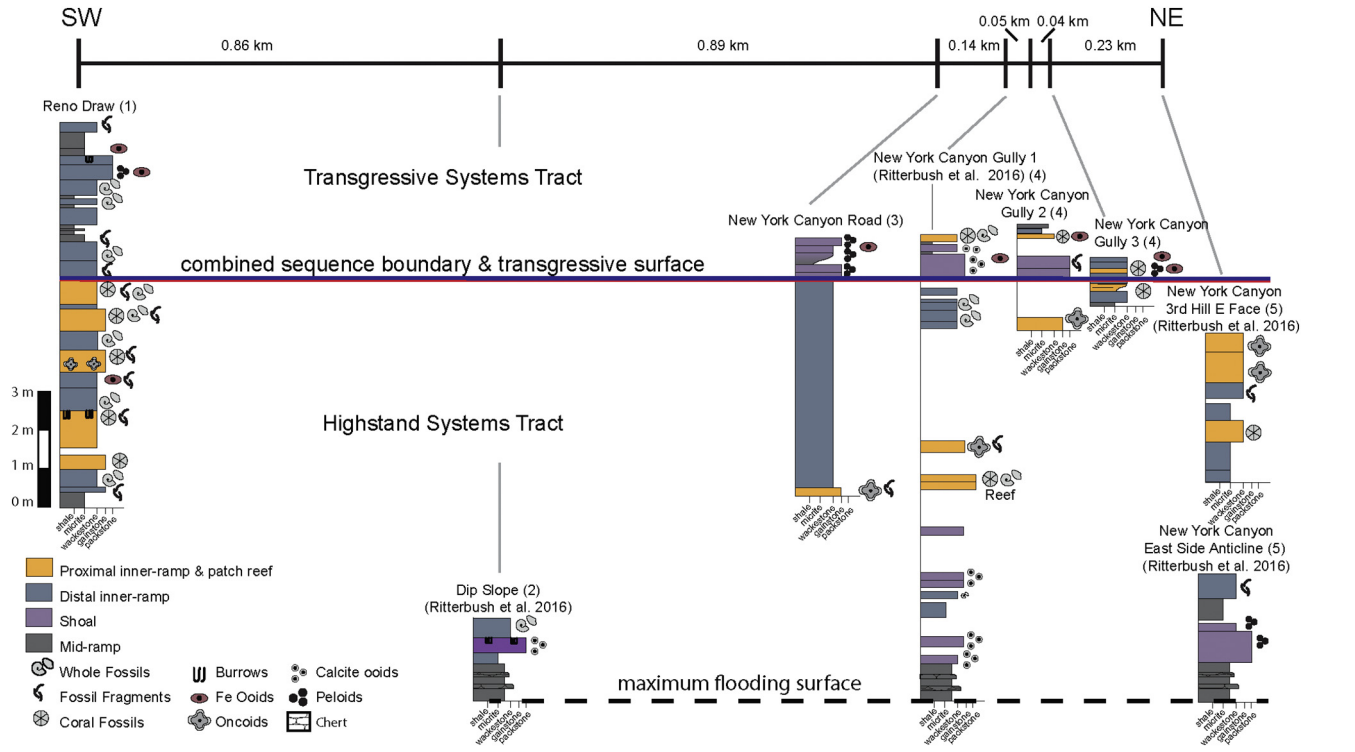

Fig. 7. Stratigraphic cross section of the Ferguson Hill Member. Stratigraphic cross section of the Ferguson Hill Member of the Sunrise Formation with sequence stratigraphic interpretation.

of sediments in a deposit (Föllmi, 2016). The accumulation of iron, which is usually oxidized or biologically scavenged, can produce authigenic mineral formation in stratigraphically condensed sections (Embry and Johannessen, 1993; Collin et al., 2005; Föllmi, 2016). Major flooding surfaces and transgressive systems tracts are often associated with condensed section by flooding the environment to depths with low deposition, or by interrupting the production of sediment by temporarily shutting down the carbonate factory (Föllmi, 2016).

The production, transport, and preservation of iron ooids in a restricted stratigraphic interval and across multiple facies support the interpretation of a low sedimentation rate sufficient to concentrate a substantial percentage of grains in Ferguson Hill Member samples. This pattern of deposition for iron ooids is not uncommon. Oolitic ironstones from the Svedrup Basin of Canada are interpreted to occur in sediment-starved environments and are similarly found in the transgressive systems tract in deposits just above the transgressive surface in multiple sections (Embry, 1982; Embry and Johannessen, 1993). However, the Ferguson Hill Member iron ooids remain unique in that their deposition in carbonate wackestone to grainstone units does not constitute an ironstone lithology or facies interpretation.

The transgressive interval in the Ferguson Hill Member was not previously recognized. Prior work (Taylor et al., 1983) recognized the Ferguson Hill Member as a set of shallowing upward parasequences until its upper contact with the basinward siltstones of the Five Card Draw Member. Focus on the interval containing iron ooids allowed for the recognition of a change in stacking patterns from progradational to retrogradational prior to the major basinward shift of the Five Card Draw Member strata. This change in stacking pattern from shallowing upwards to a brief deepening upwards (within the defined Ferguson Hill Member) is the primary identifying feature of the combined sequence boundary and transgressive surface (Fig. 7). There is little to no noticeable erosion on the sequence boundary indicating that the seafloor was likely not subaerially exposed. The discovery of authigenic iron, in the form of iron ooids, in the strata immediately overlying the combined surface supports the interpretation that the onset of the transgression occurred within the Ferguson Hill Member rather than at the contact with the Five Card Draw Member.

The Ferguson Hill Member iron ooids remain somewhat unique among condensed section iron ooid deposits for their low density and formation on a carbonate ramp. Oolitic ironstones are often found in siliciclastic deposits (Bayer, 1989; Van Houten, 2000; Young, 1989), and when they are found in association with carbonate deposits, it is usually at a transition from carbonate to siliciclastic environments (Bayer, 1989). This contrasts with the Ferguson Hill Member iron ooids that are well-incorporated into shallow carbonate deposits. Low concentration or lean (<30%) iron ooid accumulations of low economic potential have been recognized in passing from the Phanerozoic, but few have been actively studied (Bhattacharyya, 1989). This combination of uncommon carbonate depositional system and lean iron ooid accumulation is likely why this deposit was, until recently, unnoticed. There is a high likelihood that iron ooids have been overlooked as a potential component of carbonate systems or simply not recognized in studies owing to very lean accumulations.

6.3. Iron ooid formation

Precipitation of iron aluminosilicates either directly from a fluid or from a ferruginous silica gel at low temperatures (i.e., normal ocean conditions) relies on the relative availability of the constituent molecules, pH, and the reduction potential (Harder, 1978). These physical constraints allow for inference of the geochemical conditions producing iron ooids in the Ferguson Hill Member. Of the numerous proposed mechanisms of iron ooid formations (Kimberley, 1974; Harder, 1978; Bhattacharyya, 1983; Van Houten and Purucker, 1984; Kearsley, 1989; Siehl and Thein, 1989; Young, 1989; Collin et al., 2005; Di Bella et al., 2019), two of the most likely scenarios for the Ferguson Hill Member iron ooids will be examined: accretionary growth of iron-rich clays, and micro-concretionary growth at or near the sediment-water interface.

6.3.1. Mechanical accretion of iron-rich phases and/or mechanical accretion of clays with subsequent transformation to iron-rich phases

Mechanical accretion of iron-rich phases or clays follow a classic "snow ball" model where particles are accreted by rolling action that

builds up cortical layers around a central core (Bhattacharyya, 1983; Young, 1989). This process would likely leave a tangential orientation of clay particles in the cortical layers (Kearsley, 1989); however, little evidence of tangential orientation has been observed in microstructure analyses of ferruginous ooids in the Ferguson Hill Member (Fig. 6) or elsewhere. A model of mechanical accretion also requires the development of precursor clays, such as kaolinite (Bhattacharyya, 1983), which are not observed in Ferguson Hill Member iron ooids. Precursor clays, such as kaolinite, are not found in ooids without transformation to iron-rich phases (Young, 1989). The transformation from kaolinite to iron-rich phases, such as chamosite, may also destroy accretionary fabrics, leaving little evidence of their original formation (Van Houten and Bhattacharyya, 1982; Young, 1989).

Ferguson Hill iron ooids did not show any orientation of iron-rich phases in SEM analysis; rather, their microstructure was distinctly clotted and mixed largely with amorphous silica (Fig. 6). Lacking tangential clay orientation or evidence of precursor clays, an accretionary formation mechanism has little support from direct evidence in the Ferguson Hill Member or generally among ferruginous ooid deposits.

6.3.2. In situ growth as micro-concretions

Marine ferruginous ooids' textural similarities to pedogenic ooids suggest a formational mechanism of micro-concretion growth (Hallimond, 1925; Hemingway, 1974). This largely intrasedimentary mechanism relies on in situ fluctuation in chemical conditions to create the cortical layers similar to pedogenic calcite ooid formation (Hallimond, 1925; Hemingway, 1974; Young, 1989) (Fig. 8). Iron-clay mineral deposition requires a reducing environment (Harder, 1978, 1989) that silica and calcite do not. Therefore, fluctuations in the oxidizing/reducing (redox) conditions during iron ooid formation are likely responsible for the alternating mineralogy of the cortical layers. Fluctuation of oxidizing/reducing conditions in pore water and at the sediment-water interface can be produced in several ways. Short-term variation can arise from physical reworking between the sediment and the water column (Young, 1989). The position of the oxidation/reduction transition within the sediment can be altered by changes in bioturbation and the addition or removal of overlying sediments. Physical reworking producing repeated burial and exposure can also cause variation in chemical environments (Young, 1989). However, it is unclear whether the concentric nature of the cortical layers is produced entirely by the change in chemical conditions at the time of formation (Chauvel and Guerrak, 1989), or if their concentric nature arises from differential diagenetic processes acting upon and concentrating differing mineralogies within the iron ooid (Kearsley, 1989). In either case, cortical layers in iron ooids usually lack the radial mineral structure found in pedogenic calcite ooids (Bhattacharyya, 1983; Young, 1989), allowing calcitic and iron ooids to be differentiated on appearance and formational process.

A redox-controlled micro-concretionary growth model agrees with textural evidence from the Ferguson Hill Member iron ooids. Evidence of iron ooid reworking that could induce redox changes includes a lack of long axis orientation and deformed or damaged iron ooids that retain some cortical layers (Fig. 3c, d), indicating that the ooids were formed and deposited with cortical layers intact and then sustained damage from subsequent exposure. The retention of cortical layers in damaged ooids supports fluctuating chemical environments to be the source of cortical layers original structure rather than post-depositional diagenetic processes (Kearsley, 1989; Van Houten and Bhattacharyya, 1982; Young, 1989) (Fig. 8). The cortical layers must have existed before burial of damaged ooids and their original nature has not been overprinted by significant diagenetic processes. The clotted texture of iron-rich phases (iron aluminosilicates) in SEM suggests some potential diagenetic migration of amorphous silica; however, distinct cortical layers visible in transmitted light microscopy show that phases are not so mixed or remineralized that original structure is lost.

This micro-concretionary growth model contrasts significantly with the proposed formation of modern iron ooids. A recent study by Di Bella et al. (2019) describes an active deposit of iron ooids near a volcanic island north of Sicily, Italy. The modern iron ooids are accumulating in an area of significant hydrothermal activity at a depth of 80 m (Di Bella et al., 2019); a much different environment than the likely shallow waters of a mid- to inner- carbonate ramp in the Ferguson Hill Member. Modern iron ooids cortical layers are composed entirely of the iron oxyhydroxide, goethite (FeO(OH)) (Di Bella et al., 2019) and show no alternating cortical layers of iron and silica. Hydrothermal exhalation is the source of both iron and dissolved silica in this modern setting. The warm rising hydrothermal fluid mixes with seawater near the sediment-water interface above the redox boundary and initiates iron mineral deposition around seafloor sediments. Cortical layers classic to iron ooids are a result of periodic remobilization by wave action (Di Bella et al., 2019). The lack of oxidized iron minerals and the presence of silica and calcite cortical layers in the Ferguson Hill Member iron ooids indicate their formation process differed from modern iron ooids. While both processes call for concentrated iron and silica near the sediment-water interface and periodic remobilization, the formation of iron-clay minerals requires a reducing environment (Harder, 1978, 1989) that is less likely to produce goethite.

6.4. Sources of silica

The availability of silica is integral to the formation of aluminosilicates, and unique conditions in the early Jurassic may explain the formation of iron ooids in a shallow carbonate system. In today's seas, potential sources of dissolved silica (siliceous acid) arrive from runoff over weathered continental rocks and terrestrial basalts; from deep-sea hydrothermal vents; and throughout the water column via remobilization of biogenic opal (e.g., Tréguer et al., 1995; DeMaster, 2002). Strontium isotope chemostratigraphy of the Triassic–Jurassic transition supports interpretations of increased silica flux to the ocean over approximately six million years (Ritterbush et al., 2015). Global composite $^{87}Sr/^{86}Sr$ ratios for the Rhaetian into the early Jurassic show a shift to lighter values, which have been attributed to increased hydrothermal input, or weathering of

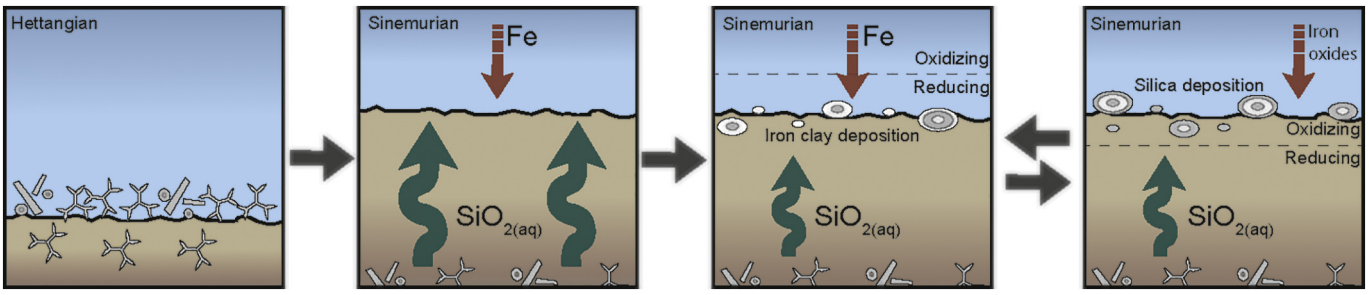

Fig. 8. Schematic diagram of ooid formation. Schematic diagram depicting the proposed redox fluctuations necessary to produce the Ferguson Hill Member iron ooids. Silica is sourced from dissolved biogenic silica in buried sediments enriching pore waters. In reducing conditions when the redox boundary is at or above the sediment-water interface iron and silica will tend to form iron clay minerals. In oxidizing conditions when the redox boundary is below the sediment-water interface amorphous silica and iron oxides tend to form.

basalts associated with the onset of Central Atlantic Magmatic Province (CAMP) volcanism (Callegaro et al., 2012; Korte et al., 2004). A record of this isotopic shift is well-documented through the Upper Triassic Luning and Gabbs Formation strata in New York Canyon, Nevada (Tackett et al., 2014). The negative trend is interrupted by a brief plateau in values in the earliest Jurassic (Hettangian), consistent with a large influx of continental sediments related to continental rifting (Callegaro et al., 2012). Next, the Sr record resumes a negative trend which has been interpreted as increased flux rates of basaltic weathering products (Jones et al., 1994). Ritterbush et al. (2014) estimated that intense weathering of CAMP basalts could have supplied sufficient siliceous acid to support the Hettangian and early Sinemurian proliferation of dense siliceous sponge meadows.

The aluminosilicate ooid contents may have also been supported by a flux of silica in pore waters, or hyperlocal marine water, from remineralization of silica from detrital sponge spicules. Biogenic opal (amorphous and hydrated) has a greater solubility than crystalline (quartz) silica, and the solubility is further increased by the high surface area of siliceous microfossils such as sponge spicules (Faure, 1991; Quéguiner, 2016; Williams et al., 1985). Biogenic silica dissolution typically occurs in pore waters after deposition then is typically exported upwards within the sediment column, making dissolved silica available to overlying sediments or, if shallow enough, to the sediment-water interface and overlying marine water (Tréguer et al., 1995; DeMaster, 2002; Quéguiner, 2016). Siliceous sponge spicules are ubiquitous as in situ sponge meadows and as detrital sediments throughout the Ferguson Hill Member of the Sunrise Formation (Hettangian and Lower Sinemurian) (Ritterbush et al., 2014). Although the in situ sponge meadows are not observed in the uppermost strata of the Ferguson Hill Member, detrital spicules and reworked intraclasts of spicule-microbe mat are well-represented in the upper strata (Ritterbush et al., 2016), suggesting that they persisted as important biosediments throughout the early Jurassic, and are the likely source for dissolved silica for the iron ooids (Fig. 8).

6.5. Role of the silicon cycle

The precipitation of an iron-aluminosilicate (iron-clay mineral) grain in shallow marine settings naturally raises the question of its role in the biogeochemical cycling of silicon in the ocean. This topic has not been directly addressed by previous work, but the potential for fluctuating pore fluid chemistry (Young, 1989), the prominent silica layers in the Ferguson Hill Member iron ooids, and laboratory experiments on the precipitation of chamosite suggest a connection (Harder, 1978). Biogenic silica from sponges was a significant sedimentary input in the Hettangian and early Sinemurian of the New York Canyon area (Ritterbush et al., 2014), and biological uptake by sponges contributed to cycling during this interval (Maldonado et al., 2011; Ritterbush et al., 2014). Weathering of CAMP basalts has been proposed as the original source of silica for sponges in the early Jurassic (Ritterbush et al., 2014). Despite the availability of dissolved silica from CAMP volcanism and likely pore-water dissolution of sponge spicules, sedimentary deposits containing iron ooids are not observed until the middle of the Ferguson Hill Member (Ritterbush et al., 2016). The deposition of abiotic silica in the Ferguson Hill iron ooids suggests additional abiotic processes contributed to the cycling of silicon during carbonate recovery in the Sinemurian.

The presence of iron ooids in primarily carbonate facies also provides a useful modeling proxy for carbonate systems. Iron ooids associated with carbonates are usually found in mixed systems or where carbonate sediments transition into siliciclastic sediments (Bayer, 1989). The Ferguson Hill iron ooids are found well incorporated into shallow carbonate facies OC, SLMG, and CWPO. Constraining the geochemistry of carbonate systems may allow for the detection of a relatively rare confluence of conditions capable of producing iron ooids, conditions which may have been present following the carbonate crisis of the latest Triassic.

6.6. Comparison to other early Jurassic ironstones

6.6.1. Minette-type European ironstones

Minette-type ironstones are perhaps the most recognized form of oolitic ironstone deposit (Hallam and Bradshaw, 1979; Siehl and Thein, 1989; Teyssen, 1984). They are oolitic, thought to be detrital in origin, and can contain a variety of mineralogies including aluminous goethite, hematite, and aluminum-rich berthierine/chamosite (Siehl and Thein, 1989). Accumulation of iron ooids occurred primarily in thick, tidally-driven, sand wave deposits, seaward of a deltaic system (Teyssen, 1984). Owing to the apparently limited depositional environment in which Minette-style iron ooids form (Teyssen, 1984) and the variable mineralogy (Siehl and Thein, 1989), these are unlikely to be an appropriate analogue to the iron ooids formed in the Ferguson Hill Member.

6.6.2. Svedrup Basin ironstones

The Svedrup Basin of Canada has several ironstone intervals within a primarily siliciclastic succession of similar age to the Ferguson Hill Member. Oolitic ironstone deposits are interpreted as transgressive strata that form in two distinct environments in a deltaic siliciclastic system, a starved shallow shelf and semi-starved offshore shelf (Embry, 1982; Embry and Johannessen, 1993). Embry and Johannessen (1993) also suggest these environments may have experienced abnormal levels of salinity owing to a lack of bioturbation in both environments.

The environments for iron ooid deposition, and potentially their formation, vary greatly between the Svedrup Basin siliciclastic delta and the Ferguson Hill Member carbonate ramp, suggesting that redox conditions are likely to have exerted greater control over iron ooid deposition than grain mineralogy. Salinity as well as temperature, pH, and dissolved silica and iron content all likely contributed to geochemical conditions capable of producing iron ooids. Changes in sediment deposition during transgressions often produce fluctuations in the position of the oxidation/reduction zone within sediments and can produce the dysoxic conditions that are arguably necessary for reducing conditions to form unoxidized iron aluminosilicates (Föllmi, 2016). Iron ooids formed in an array of environments as noted by Bayer (1989); however, Bayer (1989) also suggests that widespread ironstones predominantly accumulated in marginal bar deposits and likely formed in lagoonal settings. The relative scarcity of iron ooids in the Ferguson Hill Member compared to true ironstones implies that the physical and potentially chemical environment that produced iron ooids was not ideal for widespread ironstone formation.

7. Conclusions

The iron ooids found in the Ferguson Hill Member are morphologically distinct from calcite ooids, and present multiple features which allow them to be recognized in the field and in thin-section. Iron ooids are ovate (oblate, prolate, and triaxial) rather than spherical and show laminae that thicken on long axes. Though cortical laminae are present in Ferguson Hill Member iron ooids, laminae are commonly composed of an iron-clay mineral (chamosite or berthierine) and amorphous silica and only rarely composed of carbonate. Iron ooids visible in hand sample may appear a bright white that stands out from the host of tan limestone owing to the iron-clay mineral laminae.

Iron ooids formed in a wide range of depositional environments, unlike their calcite counterparts, indicating their formation was likely controlled more by the geochemical rather than the physical environment. In the Ferguson Hill Member, iron ooids are found in sedimentary deposits interpreted to be oolitic shoal, distal inner-ramp, proximal inner-ramp and patch reef, and environments. Their abundance and frequently undamaged nature indicate the iron ooids formed in or very near these shallow marine carbonate environments. The formation of iron ooids appears more sensitive to geochemical fluctuations than physical environment.

The sequence stratigraphic interpretation indicates that iron ooids formed as a condensation feature within the transgressive systems tract of a carbonate ramp environment. In this context, iron ooids may represent a useful, and potentially overlooked, proxy in carbonate systems for elucidating redox and silica cycles during major perturbations, which are thought to have been well underway in the latest Triassic — earliest Jurassic. Significant shifts in silica weathering and ocean acidification are recognized in the latest Triassic mass extinction interval, and in its aftermath. Thus, the combination of sequence stratigraphic framework, sedimentology, and paleontology provide a more nuanced understanding of the local and global geochemical conditions producing iron ooids along a depth transect in a carbonate system.

Declaration of competing interest

The authors declare that they have no known competing financial interests or personal relationships that could have appeared to influence the work reported in this paper.

Acknowledgments

This research was also supported by the National Science Foundation (NSF) [CAREER Award #1654088], and the Geological Society of America [Graduate Student Research Grant]. The SEM and elemental analyses in this manuscript are based upon work supported by the National Science Foundation [Award #0619098]. The authors would like to thank Joyce Yager, Haley Marston, Sara Gibbs-Schnucker, and Kaitlyn Fleming for field assistance as well as Sam Marolt, Joel Schock, and Rodney Utter for lab assistance.

References

Basso, D., Bracchi, V.A., Favalli, A.N., 2012. Microbialite formation in southern Sinai (Egypt). Facies 58, 70–18.
Bayer, U., 1989. Stratigraphic and environmental patterns of ironstone deposits. In: Young, T.P., Taylor, W.E.G. (Eds.), Phanerozoic Ironstones. Geological Society of London Special Publication 46, London, pp. 105–117.
Bhattacharyya, D.P., 1983. Origin of berthierine in ironstones. Clay Clay Miner. 31, 173–182.
Bhattacharyya, D., 1989. Concentrated and lean oolites: examples from the Nubia Formation at Aswan, Egypt, and significance of the oolite types in ironstone genesis. In: Young, T.P., Taylor, W.E.G. (Eds.), Phanerozoic Ironstones. Geological Society of London Special Publication 46, London, pp. 93–103.
Burchette, T.P., Wright, V.P., 1992. Carbonate ramp depositional systems. Sediment. Geol. 79, 3–57.
Callegaro, S., Rigo, M., Chiaradia, M., Marzoli, A., 2012. Latest Triassic marine Sr isotopic variations, possible causes and implications. Terra Nova 24, 130–135.
Chauvel, J.J., Guerrak, S., 1989. Oolitization processes in Palaeozoic ironstones of France, Algeria and Libya. In: Young, T.P., Taylor, W.E.G. (Eds.), Phanerozoic Ironstones. Geological Society of London Special Publication 46, London, pp. 165–173.
Collin, P., Loreau, J., Courville, P., 2005. Depositional environments and iron ooid formation in condensed sections (Callovian–Oxfordian, south-eastern Paris basin, France). Sedimentology 52, 969–985.
Dahanayake, K., Krumbein, W.E., 1986. Microbial structures in oolitic iron formations. Mineral. Deposita 21, 85–94.
DeMaster, D.J., 2002. The accumulation and cycling of biogenic silica in the Southern Ocean: revisiting the marine silica budget. Deep-Sea Res. II Top. Stud. Oceanogr. 49, 3155–3167.
Di Bella, M., Sabatino, G., Quartieri, S., Ferretti, A., Cavalazzi, B., Barbieri, R., Foucher, F., Messori, F., Italiano, F., 2019. Modern iron ooids of hydrothermal origin as a proxy for ancient deposits. Scientific Reports 9(1), 7107, doi:https://doi.org/10.1038/s41598-019-43181-y.
Embry, A.F., 1982. The Upper Triassic-Lower Jurassic Heiberg deltaic complex of the Sverdrup Basin. In: Embry, A.F., Balkwill, H.R. (Eds.), Arctic Geology and Geophysics: Proceedings of the Third International Symposium on Arctic Geology. vol. 8, pp. 189–217 Geological Society of Petroleum Geologists Memoir.
Embry, A.F., Johannessen, E., 1993. T–R sequence stratigraphy, facies analysis and reservoir distribution in the uppermost Triassic–Lower Jurassic succession, western Sverdrup Basin, Arctic Canada. In: Vorren, T.O., Bergsager, E., Dahl-Stamnes, Ø.A., Holter, E., Johansen, B., Lie, E., Lund, T.B. (Eds.), Arctic Geology and Petroleum Potential. Norwegian Petroleum Society Special Publications, Elsevier, Amsterdam, pp. 121–146.
Faure, G., 1991. Principles and Applications of Inorganic Geochemistry: A Comprehensive Textbook for Geology Students. Prentice Hall, New Jersey.
Ferguson, H.G., Muller, S.W., 1949. Structural geology of the Hawthorne and Tonopah quadrangles, Nevada. Geological Survey Professional Paper 216. Office. Washington D.C., US Government Printing.
Föllmi, K.B., 2016. Sedimentary condensation. Earth Sci. Rev. 152, 143–180.
Greene, S.E., Martindale, R.C., Ritterbush, K.A., Bottjer, D.J., Corsetti, F.A., Berelson, W.M., 2012. Recognizing ocean acidification in deep time: an evaluation of the evidence for acidification across the Triassic-Jurassic boundary. Earth-Sci. Rev. 113, 72–93.
Hallam, A., Bradshaw, M.J., 1979. Bituminous shales and oolitic ironstones as indicators of transgressions and regressions. J. Geol. Soc. 136, 157–164.
Hallimond, A.F., 1925. Iron Ores: Bedded Ores of England and Wales: Petrography and Chemistry. HM Stationery Office, London, p. 29.
Harder, H., 1978. Synthesis of iron layer silicate minerals under natural conditions. Clay Clay Miner. 26, 65–72.
Harder, H., 1989. Mineral genesis in ironstones: a model based upon laboratory experiments and petrographic observations. In: Young, T.P., Taylor, W.E.G. (Eds.), Phanerozoic Ironstones. Geological Society of London Special Publication 46, London, pp. 9–18.
Heim, A., 1934. Stratigraphische Kondensation. Eclogae Geol. Helv. 27, 372–383.
Hemingway, J.E., 1974. Jurassic. In: Raynor, D.H., Hemingway, J.E. (Eds.), The Geology and Mineral Resources of Yorkshire. Yorkshire Geological Society, The Geological of London, London, pp. 161–223.
Jones, C.E., Jenkyns, H.C., Hesselbo, S.P., 1994. Strontium isotopes in Early Jurassic seawater. Geochim. Cosmochim. Acta 58, 1285–1301.
Kearsley, A., 1989. Iron-rich ooids, their mineralogy and microfabric: clues to their origin and evolution. In: Young, T.P., Taylor, W.E.G. (Eds.), Phanerozoic Ironstones. Geological Society of London Special Publication 46, London, pp. 141–164.
Kimberley, M.M., 1974. Origin of iron ore by diagenetic replacement of calcareous oolite. Nature 250, 319.
Korte, C., Kozur, H.W., Joachimski, M.M., Strauss, H., Veizer, J., Schwark, L., 2004. Carbon, sulfur, oxygen and strontium isotope records, organic geochemistry and biostratigraphy across the Permian/Triassic boundary in Abadeh, Iran. Int. J. Earth Sci. 93, 565–581.
Maldonado, M., Cao, H., Cao, X., Song, Y., Qu, Y., Zhang, W., 2011. Experimental silicon demand by the sponge *Hymeniacidon perlevis* reveals chronic limitation in field populations. In: Maldonado, M., Turon, X., Becerro, M.A., Uriz, M.J. (Eds.), Ancient Animals, New Challenges. Springer, New York, pp. 251–257.
Middleton, G.V., 1973. Johannes Walther's law of the correlation of facies. Geol. Soc. Am. Bull. 84, 979–988.
Powers, M.C., 1953. A new roundness scale for sedimentary particles. J. Sediment. Res. 23, 117–119.
Quéguiner, B., 2016. The Biogeochemical Cycle of Silicon in the Ocean. John Wiley and Sons, New Jersey.
Rankey, E.C., Riegl, B., Steffen, K., 2006. Form, function and feedbacks in a tidally dominated ooid shoal, Bahamas. Sedimentology 53, 1191–1210.
Ritterbush, K.A., Bottjer, D.J., Corsetti, F.A., Rosas, S., 2014. New evidence on the role of siliceous sponges in ecology and sedimentary facies development in Eastern Panthalassa following the Triassic–Jurassic mass extinction. Palaios 29, 652–668.
Ritterbush, K.A., Rosas, S., Corsetti, F.A., Bottjer, D.J., West, A.J., 2015. Andean sponges reveal long-term benthic ecosystem shifts following the end-Triassic mass extinction. Palaeogeogr. Palaeoclimatol. Palaeoecol. 420, 193–209.
Ritterbush, K.A., Ibarra, Y., Tackett, L.S., 2016. Post-extinction biofacies of the first carbonate ramp of the Early Jurassic (Sinemurian) in NE Panthalassa (New York Canyon, Nevada, USA). Palaios 31, 141–160.
Schaller, M.F., Wright, J.D., Kent, D.V., 2015. A 30 Myr record of Late Triassic atmospheric pCO_2 variation reflects a fundamental control of the carbon cycle by changes in continental weathering. Geol. Soc. Am. Bull. 127, 661–671.
Schoene, B., Guex, J., Bartolini, A., Schaltegger, U., Blackburn, T.J., 2010. Correlating the end-Triassic mass extinction and flood basalt volcanism at the 100 ka level. Geology 38, 387–390.
Siehl, A., Thein, J., 1989. Minette-type ironstones. In: Young, T.P., Taylor, W.E.G. (Eds.), Phanerozoic Ironstones. Geological Society of London Special Publication 46, London, pp. 175–193.
Simone, L., 1981. Ooids: a review. Earth Sci. Rev. 16, 319–355.
Tackett, L.S., Kaufman, A.J., Corsetti, F.A., Bottjer, D.J., 2014. Strontium isotope stratigraphy of the Gabbs Formation (Nevada): implications for global Norian–Rhaetian correlations and faunal turnover. Lethaia 47, 500–511.
Taylor, D.G., Smith, P.L., Laws, R.A., Guex, J., 1983. The stratigraphy and biofacies trends of the Lower Mesozoic Gabbs and Sunrise formations, west-central Nevada. Can. J. Earth Sci. 20, 1598–1608.
Teyssen, T., 1984. Sedimentology of the Minette oolitic ironstones of Luxembourg and Lorraine: a Jurassic subtidal sandwave complex. Sedimentology 31, 195–211.
Tréguer, P., Nelson, D.M., Van Bennekom, A.J., DeMaster, D.J., Leynaert, A., Quéguiner, B., 1995. The silica balance in the world ocean: a reestimate. Science 268, 375–379.
Tucker, M.E., 1985. Shallow-marine carbonate facies and facies models. In: Brenchley, P.J., Williams, B.P.J. (Eds.), Sedimentology Recent Developments and Applied Aspects. Geological Society of London Special Publications 18, London, pp. 147–169.
Van Houten, F.B., 1985. Oolitic ironstones and contrasting Ordovician and Jurassic paleogeography. Geology 13, 722–724.
Van Houten, F.B., 2000. Ooidal ironstones and phosphorites—a comparison from a stratigrapher's view. In: Glenn, C.R., Prévôt-Lucas, L., Lucas, J. (Eds.), Marine Authigenesis: From Global to Microbial. SEPM Special Publication 66, Oklahoma, pp. 127–132.
Van Houten, F.B., Arthur, M.A., 1989. Temporal patterns among Phanerozoic oolitic ironstones and ocean anoxia. In: Young, T.P., Taylor, W.E.G. (Eds.), Phanerozoic Ironstones. Geological Society of London Special Publication 46, London, pp. 33–49.
Van Houten, F.B., Bhattacharyya, D.P., 1982. Phanerozoic oolitic ironstones–geologic record and facies model. Annu. Rev. Earth Planet. Sci. 10, 441–457.

Van Houten, F.B., Hou, H.-F., 1990. Stratigraphic and palaeogeographic distribution of Palaeozoic oolitic ironstones. In: McKerrow, W.S., Scotese, C.R. (Eds.), Palaeozoic Palaeogeography and Biogeography. Geological Society of London Memoirs 12, London, pp. 87–93.

Van Houten, F.B., Purucker, M., 1984. Glauconitic peloids and chamositic ooids-favorable factors, constraints, and problems. Earth Sci. Rev. 20, 211–243.

Williams, L.A., Parks, G.A., Crerar, D.A., 1985. Silica diagenesis; I, solubility controls. Journal of Sedimentary Research 55, 301–311.

Young, T.P., 1989. Phanerozoic ironstones: an introduction and review. In: Young, T.P., Taylor, W.E.G. (Eds.), Phanerozoic Ironstones. Geological Society of London Special Publication 46, London, pp. ix-xxv.